

Nonlinear optical spectroscopy of soft matter interfaces

Sylvie Roke

Max-Planck Institute for Metals Research

Heisenbergstrasse 3, 70569 Stuttgart, Germany, roke@mf.mpg.de

24th April 2009

Abstract

Soft matter consists of complex molecules that can undergo drastic structural transformations under mild changes of chemical and physical conditions. Since a wide variety of chemical, physical and biological processes occur at soft matter interfaces, they can exhibit complex behavior. This is even more so for interfaces of colloidal soft matter since the relative amount of interface material increases by orders of magnitude. This minireview focuses on new developments that enable us to obtain detailed molecular structural changes in the topmost molecular layers of soft matter interfaces composed of complex bio-molecules. In particular, we will discuss possibilities to probe interfaces of colloidal soft matter systems.

keywords: bio-interfaces, soft matter interfaces, sum frequency scattering, second harmonic scattering, colloids, gelation, chirality

1 Introduction

Soft matter refers to materials whose stabilizing interactions occur in the energy range of kT_c . Therefore, even at room temperature (T_c), subtle changes in composition, chemistry, pressure or temperature can strongly influence the physical or chemical properties of soft matter systems. Most biological and biologically relevant matter can be identified with the term soft matter and it is therefore not surprising that an enormous diversity of biochemical processes exist in nature.

Apart from studying the diverse properties of bulk soft matter systems, in the past century scientists have also uncovered many important properties of their interfaces (see e.g. [1,2]). Surfaces and interfaces are often facilitating (the start of) chemical and physical changes and this function becomes more important if the size of matter is decreased from macroscopic proportion down to the micro- and nanometer scale.

During the last decades nonlinear optical surface spectroscopy has played an important role in uncovering the molecular mechanism behind many interfacial phenomena. In this minireview, we will first discuss recent advances in the area of surface nonlinear optics that are specifically aimed towards obtaining detailed understanding of the functionality of biologically relevant molecules at interfaces. Next we will make the transition to colloidal soft matter, by first discussing some theoretical background on nonlinear light scattering methods. These methods enable us to obtain surface molecular properties of colloidal particles dispersed in liquids and solid matrices, which will be discussed next.

2 Vibrational sum frequency generation as a tool for soft matter interfaces

A molecular picture of an interface can be obtained by using nonlinear surface spectroscopy. The two most common methods are Second Harmonic Generation (SHG) and Sum Frequency Generation (SFG) [3]. In an SHG experiment a visible (VIS) beam is reflected from a surface. At the surface two photons are combined into one photon with the double, Second Harmonic (SH), frequency. Usually, the SH photons are at resonance with an electronic transition of the surface molecules. In this

minireview we will put most emphasis on vibrational sum frequency generation, because of its direct sensitivity to chemical bonds. Here, two electromagnetic fields, $\mathbf{E}_1(\mathbf{r}, t) = \mathcal{E}_1 \mathbf{u}_1 e^{i(\mathbf{k}_1 \cdot \mathbf{r} - \omega_1 t)}$ and $\mathbf{E}_2(\mathbf{r}, t) = \mathcal{E}_2 \mathbf{u}_2 e^{i(\mathbf{k}_2 \cdot \mathbf{r} - \omega_2 t)}$, with amplitudes \mathcal{E}_1 and \mathcal{E}_2 , polarization states \mathbf{u}_1 and \mathbf{u}_2 , and frequencies ω_1 and ω_2 , are reflected from an interface¹. The frequency of the field \mathbf{E}_2 is tuned around the resonance of the vibrational modes of the interfacial molecules, so that the wavenumbers will be in the range of 3700 - 1000 cm^{-1} . The other electromagnetic field is usually kept at a fixed visible wavelength (usually 532 or 800 nm, which are readily available from ns, ps, or fs pulsed laser sources). At the interface a second-order polarization can be created that oscillates at the sum frequency of the incoming waves:

$$\mathbf{P}_i^{(2)}(\omega_0 = \omega_1 + \omega_2) = \chi_{ijk}^{(2)}(\omega_0 = \omega_1 + \omega_2) \mathbf{E}_{1,j}(\omega_1) \mathbf{E}_{2,k}(\omega_2) \quad (1)$$

whose size and spectral shape is determined by the second-order susceptibility tensor $\chi^{(2)}$. Since $\chi^{(2)}$ is a physical property of the material it must reflect also the spatial symmetry properties of that material (Neumann's principle). As a consequence (in the electric-dipole approximation) $\chi_{ijk}^{(2)}$ vanishes in bulk media [4]. This means that SFG can often be applied as a surface specific technique, with which only the first few molecular layers situated at the interface are probed. The surface response, identified as $\chi_s^{(2)}$, is usually split up in a frequency dependent resonant (*res*) and a frequency independent non-resonant (*nr*) response:

$$\chi_{s,ijk}^{(2)} = \chi_{s,nr,ijk}^{(2)} + \chi_{s,res,ijk}^{(2)} \propto A_{nr} e^{i\Delta\phi} + \sum_n \frac{N_s \langle T_{ia} T_{jb} T_{kc} \rangle R_{n,ab} \mu_{n,c}}{\hbar(\omega_2 - \omega_{0n} + i\Upsilon_{0n})} \quad (2)$$

where n refers to a specific vibrational mode, with resonance frequency ω_{0n} , and damping constant Υ_{0n} . This equation relates the resonant surface susceptibility $\chi_{s,res}^{(2)}$ to the hyperpolarizability tensor $\beta_n^{(2)}$ which is the product of the vibrational dipole moment μ_n with the Raman polarizability \mathbf{R}_n through a transformation matrix \mathbf{T} that transforms from the molecular coordinate frame (a, b, c) to the surface coordinate frame (i, j, k). N_s is the density of surface molecules. A_{nr} is the amplitude of the frequency independent non-resonant response that can be phase lagged with a factor $\Delta\phi$ with respect to the resonant response. The values of ω_{0n} , Υ_{0n} , μ_n , and \mathbf{R}_n depend on the type of

¹Note that expressions for SHG can be obtained by taking $\omega_1 = \omega_2$ and $\mathbf{k}_1 = \mathbf{k}_2$

molecules, their orientation, chirality and order (see e.g. [5–7]). Since this type of information is often exclusively interface specific and can be obtained non-invasively and label-free, SFG experiments can be a useful addition to methods that are sensitive to (e.g.) average structure and mass changes. Since the first demonstrations of vibrational sum frequency generation, published in 1987 by Guyot-Sionnest et al. [8] and Harris et al. [9] many experiments have been performed using this method. Thanks to the work of many researchers the method has evolved from an exotic tool, used by only a few devoted laser experts to study model systems, to a tool that can be used by many for a diverse number of applications. Nowadays a large number of research groups are using vibrational SFG to probe such diverse aspects as optical properties [7, 10–12], structure, kinetics and dynamics [13, 14] of solid/solid, solid/liquid [5, 15], solid/gas [16, 17], liquid/liquid [18, 19], liquid/gas interfaces [20–22] and chiral media and interfaces [23–25] (note that these references are all reviews).

In the past few years some interesting developments have taken place that are aimed at extracting detailed molecular information from biologically relevant soft matter interfaces. Such interfaces are typically composed of a mixture of large molecules that have a delicate interaction balance with the surroundings. Understanding them on the molecular level is therefore a formidable task. Despite this challenge workers have begun to investigate interfaces with biopolymers (such as DNA) [26–33], phospholipids [34–40] and proteins [41–44]. As an example, it has been shown that the effect of ions on the ordering of phospholipid monolayers can be probed with high sensitivity. Fig. 1 shows the effect of Ca^{2+} ions on the ordering of phospholipid chains on water. The chain order can be probed by monitoring the ratio of the signals of the symmetric CH_3 and CH_2 stretch vibrational modes. An ordered monolayer consists of stretched alkyl chains in an all-trans conformation, that gives rise to a large signal of the symmetric CH_3 stretch modes, combined with a low or vanishing signal of the symmetric CH_2 stretch modes. A disordered monolayer will give rise to a small or vanishing signal of the symmetric CH_3 stretch modes and a relatively large signal of the symmetric CH_2 stretch modes. Fig. 1 shows that bivalent Ca^{2+} ions can both increase and decrease the chain order, depending on the lateral pressure inside the monolayer. This is different for monovalent Na^+ ions. Another promising example (also shown in Fig. 1) that illustrates how we can obtain biologically relevant insights into membrane functionality is the measurement of flip-flop rates in supported lipid bilayers. The flip-flop mechanism strongly depends on membrane density [45], composition and

temperature [35]. Further, from SFG decay measurements it is possible to estimate the activation energy and area for inter-leaflet transport.

The continuing development of more reliable pulsed pico- and femtosecond infrared laser sources has opened up the possibility to identify alpha helices, beta sheets [42] and other secondary structures as well as their orientation [46]. Also, surface vibrational modes in the fingerprint region can be detected, so that (e.g.) sulphate groups in surfactants [47], phosphate groups in phospholipids [37] and skeletal modes in polymer backbones can be measured as well. [48, 49]

A further interesting feature of nonlinear optical methods is that they are specific towards chirality. [23–25] In chemistry and biology most compounds consist of chiral building blocks (e.g. 21 of the 22 amino acids in the human body are chiral). A change in chirality can completely change the chemical and biological function of a molecule, as it strongly influences the three dimensional structure of a compound.

Furthermore, since surfaces are often heterogeneous in their composition it is important to spatially resolve the observed structural features. The development of SFG microscopy has opened up the possibility to obtain spatial information as well [50].

Since a large portion of naturally occurring matter exists in the form of small objects, such as cells, liposomes, droplets (emulsions) or colloids, it is desirable to obtain similar detailed molecular information about interfaces of small dispersed particles. Even more so, since the relative surface area of particles is orders of magnitude larger than that of planar interfaces. In order to accomplish this aim, second-order nonlinear light scattering methods have been developed. This will be introduced in the next section.

3 Nonlinear Light Scattering: Theoretical background

In a Sum Frequency Scattering (SFS) experiment the incoming beams (here assumed as plane waves) with electric field amplitudes \mathcal{E}_{u_1} and \mathcal{E}_{u_2} , polarization directions \mathbf{u}_1 and \mathbf{u}_2 and wave vectors \mathbf{k}_1 (fixed visible frequency) and \mathbf{k}_2 (tunable infrared frequency) interact with particles dispersed in another medium. Fig. 2 gives an illustration of the in-plane scattering geometry. Note that to describe Second Harmonic Scattering (SHS) experiments we need to replace ω_2 and \mathbf{k}_2 with ω_1 and \mathbf{k}_1 . For

spatially isotropic bulk and particle material, a second-order sum frequency polarization ($\mathbf{P}^{(2)}$ ($\omega_0 = \omega_1 + \omega_2$), see Eq. 1) will exclusively be generated at the particle/bulk medium interface. Just as on a planar interface $\mathbf{P}^{(2)}$ gives rise to a sum frequency field. Because we are dealing with (spherical) particles in the size range $\sim 10 \text{ nm} - 10 \text{ }\mu\text{m}$ that are typically much smaller than the incoming laser beams, and on the size scale of the wavelength of the incoming beams, the electric field components will have a different amplitude and phase at different points (\mathbf{r}') on the particle surface. As a result there is a complex near field distribution at the surface, which radiates in a wide angular distribution in the far field. The scattering angle θ is defined as the angle between the wave vector of the scattered SF photons (\mathbf{k}_0) (identical to the direction of measurement) and the direction $\mathbf{k}_1 + \mathbf{k}_2$. The angular intensity distribution of the eight possible polarization combinations ($I(\omega, \theta)_{u_0 u_1 u_2}$) are determined by the surface structure (represented by $\chi_s^{(2)}$), the particle size (given by the radius R) and shape, and the geometry of the incoming and scattered fields. SFS is therefore a direct crossover between light scattering and sum frequency generation. In analogue to linear light scattering the scattering wave vector \mathbf{q} is an important parameter. It is a function of the scattering angle and can be defined as:

$$\mathbf{q} = \mathbf{k}_0 - (\mathbf{k}_1 + \mathbf{k}_2) \quad (3)$$

$$q(\theta) = |\mathbf{q}| = 2|\mathbf{k}_0| \sin(\theta/2) \quad (4)$$

The SFS process can be described by applying the principle of time reversal of electromagnetic waves [51, 52]. For a (linear) scattering process from a surface polarization \mathbf{P} of a sphere, that emits a field \mathbf{E} that is detected at far field points \mathbf{r}_0 , the principle of time reversal states that if we reverse time, the inner product of the initial polarization \mathbf{P} with the returning time reversed field (\mathbf{E}') is identical to the inner product of the source polarization needed at \mathbf{r}_0 to create the returning field at the particle with the originally scattered field. In formulas, we have:

$$\mathbf{E}(\mathbf{r}_0) \cdot \mathbf{u}_0 = e^{ik_0 r_0} \frac{k_0^2}{r_0} \int i\omega_0 \mathbf{P} \cdot \mathbf{E}' d^3 \mathbf{r}', \quad (5)$$

where $\mathbf{E}(\mathbf{r}_0)$ is the (real) electromagnetic wave arriving in the far field with polarization direction \mathbf{u}_0 , k_0 its wave number and \mathbf{E}' is the theoretical returning (unity) plane wave from the direction of \mathbf{r}_0 . The

integration is done over the volume of the particle ($d^3\mathbf{r}'$). \mathbf{P} is the nonlinear surface polarization $\mathbf{P}^{(2)}$ that is the result of the interaction of the two incoming source fields with the surface region (given by $P_i^{(2)} = \chi_{s,ijk}^{(2)} E_{1,j} E_{2,k}$). $\mathbf{E}(r_0)$ is the sum-frequency field arriving at the detector and \mathbf{E}' is the time-reversed counterpart of \mathbf{E} (i.e. a plane wave coming in from the position of the detector with wave number k_0). The reciprocity relation then results in the following expression for the scattered sum frequency field:

$$\mathbf{E}_0(r_0) \cdot \mathbf{u}_0 = i\omega_0 e^{ik_0 r_0} \frac{k_0^2}{r_0} \int \sum_{j,k,l} E'_{0,j}(\mathbf{r}') \chi_{jkl}^{(2)}(\mathbf{r}') E_{1,k}(\mathbf{r}') E_{2,l}(\mathbf{r}') d^3\mathbf{r}', \quad (6)$$

inserting field amplitudes \mathcal{E} and polarization directions $\mathbf{u}_{1,2}$ we can introduce the effective particle susceptibility $\Gamma_{ijk}^{(2)}(\mathbf{q}, \chi^{(2)}, \mathbf{r})$ and rewrite Eq. 6 in the following form:

$$\mathcal{E}_{0,u_0,u_1,u_2}^{(2)} \propto i\omega_0 e^{ik_0 r_0} \frac{k_0^2}{r_0} \mathcal{E}_{u_1} \mathcal{E}_{u_2} \sum_{i,j,k} u_{0,i} \Gamma_{ijk}^{(2)}(\mathbf{q}, \chi^{(2)}, \mathbf{r}) u_{1,j} u_{2,k} \quad (7)$$

The intensity measured for a single vibrational or electronic surface resonance can then be written as:

$$I(\mathbf{q})_{u_0 u_1 u_2} = |\mathcal{E}^{(2)}(\mathbf{q})_{u_0 u_1 u_2}|^2 \quad \text{or} \quad I(\theta)_{u_0 u_1 u_2} = |\mathcal{E}^{(2)}(\theta)_{u_0 u_1 u_2}|^2 \quad (8)$$

where \mathbf{q} is given by Eq. 3. $\Gamma_{ijk}^{(2)}(\mathbf{q}, \chi^{(2)}, \mathbf{r})$ is the effective particle susceptibility, a convenient parameter that describes the response of the particle. Its use will be described in more detail in the next section. It contains information of the molecular orientation and order at the surface and depends both on the particle and the scattering geometry. Consequently, $\Gamma^{(2)}$ is a quantity that contains the same information contained in Eq. 2, but additionally depends on form factors that represent the shape and size of a particle [53]. Since the elements of $\chi_s^{(2)}$ appear in $\Gamma^{(2)}$ *each vibrational mode generates its own scattering pattern*. If an SFS spectrum consists of a number of vibrational modes that are close in frequency (as it typically does when C-H resonances are probed) it is necessary to first obtain the values of the vibrational amplitudes by fitting the spectra to the following equation:

$$I_{SFS}(\omega_2, \theta) \propto \left| \sum_n \mathcal{E}_2(A_{nr}(\theta) e^{i\Delta\phi} + \frac{A_n(\theta)}{(\omega_2 - \omega_{0n}) + i\Upsilon_{0n}}) \otimes \mathcal{E}_1 \right|^2, \quad (9)$$

where the indices 0, 1, 2 denote the SF, VIS and IR fields, respectively, and $A_{nr}(\theta)$ refers to the non-resonant background with relative phase $\Delta\phi$, n refers to a vibrational mode, with resonance frequency ω_{0n} , amplitude $A_n(\theta)$ and damping constant Υ_{0n} . The convolution (\otimes) with the VIS field envelope \mathcal{E}_1 is needed if the line width of the VIS field is similar to the vibrational line width. The angle dependent amplitudes obtained for a polarization combination $u_0u_1u_2$ can then be related to Eq. 8 by the following expression: $|A_n(\theta)|^2 = I_n(\theta)_{u_0u_1u_2}$. The electric field amplitudes can be found by applying the Rayleigh-Gans-Debye approximation. It assumes that the difference in dielectric constant between the particle and the bulk medium is small enough so that the beams do not distort appreciably. For soft colloidal matter this seems a reasonable assumption [54]. Defining the following form factors:

$$F_1 = 2iR^2 \left(\frac{\sin(qR)}{(qR)^2} - \frac{\cos(qR)}{(qR)} \right) \text{ and } F_2 = 4iR^2 \left(\frac{3\sin(qR)}{(qR)^4} - \frac{3\cos(qR)}{(qR)^3} - \frac{\sin(qR)}{(qR)^2} \right),$$

and abbreviated notations:

$$\chi_1 = \chi_{zzz}^{(2)} - \chi_{zxx}^{(2)} - \chi_{xzx}^{(2)} - \chi_{xxz}^{(2)}, \chi_2 = \chi_{xxz}^{(2)}, \chi_3 = \chi_{xzx}^{(2)}, \chi_4 = \chi_{zxx}^{(2)}, \text{ and}$$

$$\Gamma_1 = \Gamma_{zzz}^{(2)} - \Gamma_{zxx}^{(2)} - \Gamma_{xzx}^{(2)} - \Gamma_{xxz}^{(2)} = \pi\chi_1(2F_1 - 5F_2), \Gamma_2 = \Gamma_{xxz}^{(2)} = \pi(2F_1\chi_2 + F_2\chi_1), \Gamma_3 = \Gamma_{xzx}^{(2)} = \pi(2F_1\chi_3 + F_2\chi_1), \Gamma_4 = \Gamma_{zxx}^{(2)} = \pi(2F_1\chi_4 + F_2\chi_1),$$

the electric field components are given by:

$$E_{ppp} \propto \omega_0 e^{ik_0 r_0} \frac{k_0^2}{r_0} \Gamma_1 \cos\left(\frac{\theta}{2}\right) \cos\left(\frac{\theta}{2} - \alpha + \beta\right) \cos\left(\frac{\theta}{2} - \alpha\right) + \Gamma_4 \cos(\beta) \cos\left(\frac{\theta}{2}\right) + \Gamma_3 \cos(\theta - \alpha) \cos\left(\frac{\theta}{2} - \alpha + \beta\right) + \Gamma_2 \cos(\theta - \alpha + \beta) \cos\left(\frac{\theta}{2} - \alpha\right) \quad (10)$$

$$E_{ssp} \propto \omega_0 e^{ik_0 r_0} \frac{k_0^2}{r_0} \Gamma_2 \cos\left(\frac{\theta}{2} - \alpha\right) \quad (11)$$

$$E_{sps} \propto \omega_0 e^{ik_0 r_0} \frac{k_0^2}{r_0} \Gamma_3 \cos\left(\frac{\theta}{2} - \alpha + \beta\right) \quad (12)$$

$$E_{pps} \propto \omega_0 e^{ik_0 r_0} \frac{k_0^2}{r_0} \Gamma_4 \cos\left(\frac{\theta}{2}\right) \quad (13)$$

The RGD approximation is valid only if the refractive index ratio (m) of the bulk and particle material is close to unity and if the particles are relatively small. Apart from the RGD approximation, various other theoretical models have been worked out for SHS and SFS. In Table 1 an overview is given of the following theoretical approximations:

(i) Electrostatic approximation (for small particles), where it is assumed that the electric field is nearly

constant across the particle (ii) The Rayleigh-Gans-Debye (RGD) approximation, as discussed above (iii) The Wentzel-Kramers-Brillouin (WKB) approximation, for spheres and cylinders, where it is assumed that the a distortion of the incoming plane waves occurs only due to mismatch in velocity of the incoming beams and (iv) Mie theory for spheres, where no approximations are made. A summary of various other nonlinear light scattering phenomena can be found in Ref. [55].

3.1 Effective susceptibility and symmetry

In general, the effective particle susceptibility can be used to quickly assess whether an SHS or SFS process is allowed or not. Since $\Gamma^{(2)}$ is a physical property of both the particle and the geometry we can apply Neumann's principle to a scattering experiment, e.g. the one illustrated in Fig. 2. This is a planar scattering geometry and has therefore a horizontal mirror plane. A reflection represented by matrix R with elements $R_{ij} = (-1)^{i+1}\delta_{ij}$ should not change the outcome of the experiment. R works on Eq. 7 in the following way [4]:

$$u_{0,i}\Gamma_{ijk}^{(2)}u_{1,j}u_{2,k} = (u_{0,i}R_{ii'})(R_{i'i}\Gamma_{ijk}^{(2)}R_{jj'}R_{kk'})(R_{j'j}u_{1,j})(R_{k'k}u_{2,k}) \quad (14)$$

with $R_{ji}R_{ik} = \delta_{ik}$

The product Ru will change sign if u is polarized in the y -direction (s -polarization). The term $(R_{i'i}\Gamma_{ijk}^{(2)}R_{jj'}R_{kk'})$ will change sign only for an odd number of y indices. Thus, for an odd number of y indices Eq. 14 will be true for any value of $\Gamma_{ijk}^{(2)}$. For an even number of y indices however, Eq. 14 will be true only if $\Gamma_{ijk}^{(2)}=0$. Consequently, the only allowed polarization combinations for an SFS (or SHS) process from a non-chiral particle surface are ppp , ssp , sps and psp [54]. This is completely analogous to SFG reflection experiments.

3.2 Chiral surfaces

For spherical particles with chiral surfaces the surface susceptibility has non-zero elements of type $\chi_{xyz}^{(2)}$. These elements give rise to effective particle susceptibility of type $\Gamma_{xyz}^{(2)}$, which will emit in polarization combinations pps , spp , and psp . Since for this type of scattering the form factors are Bessel

functions of a different order than the ones in F_1 and F_2 , the angular distribution of a chiral surface pattern can be different from a non-chiral surface pattern. A comparison of scattering patterns generated by chiral and non-chiral surface structures is given in Fig. 3. Since the patterns are clearly different it should be possible to separately measure chiral and non-chiral surface responses from colloids.

4 Interfacial molecular structure of solid/liquid dispersions

Colloidal soft matter is a broad term that indicates we are dealing with particles in the size range $10 \text{ nm} \sim 10 \text{ }\mu\text{m}$ that experience low energy interactions within the kT_c range. This definition includes an enormous variety of systems that occur in nature and consists of mixtures of liquids (emulsions), micelles, vesicles, polymer particles, substances covered with liposomes, peptides, proteins etc.

Traditionally, the systems are classified in terms of the interactions that dominate between the particles. Examples are electrostatic and dispersive interactions [2]. Since the molecular interfacial properties are still relatively unexplored we will give a short overview of what has been studied and what can be studied, using nonlinear light scattering.

4.1 Sterically stabilized systems

The stability of sterically stabilized colloidal soft matter systems rely on short range repulsive interactions between the particles. Such systems occur mostly in non-aqueous media. Sterically stabilized silica particles are an example. Since they can be dispersed in apolar infrared transparent media they serve as an ideal system to test the possibilities of sum frequency scattering.

In Fig. 4 the scattering pattern and a spectrum (obtained in *ppp*-polarization) are presented of stearyl coated silica particles dispersed in CCl_4 , with radii (R) of 123 nm and 342 nm. The spectrum displays the vibrational resonances of the methyl and methylene stretch modes that are chemically bound to the particle with the purpose of providing steric stabilization. The high ratio of the CH_2 symmetric stretch amplitude vs. the CH_3 symmetric stretch amplitude indicates that the surface displays a large amount of disorder, and consequently, a low density. This contradicts elemental

analysis of the dispersion [56], which indicated that a fully packed monolayer with a molecular area of 21 \AA^2 should exist on the surfaces. Using another solvent (n-hexadecane) and making a scattering experiment with partially deuterated solvent it was found that the surface area per chain was as high as 100 \AA^2 [57]. Therefore, it is likely that during synthesis, most stearyl chains bind to the porous interior of the silica particles, and not to the surface.

The scattering pattern is displayed for a single vibrational mode (the symmetric CH_3 stretch mode) and consists of the squared amplitude of that mode. It can be obtained by globally fitting each spectrum that is obtained for each scattering angle using Eq. 9. Applying the RGD approximation [52] (Eqs. 10-14) for the different polarization combinations *ppp*, *ssp*, and *sps* allows one to extract the relative amplitude of the surface susceptibility elements. Also, it can be seen from Fig. 4 that smaller particles emit scattering patterns in a broader angular distribution.

4.1.1 Interface-solvent effects

Interestingly, when these porous surface modified silica particles are dispersed in apolar solvents at low temperature they can be in a gel state. Upon heating, the dispersion changes from a solid-like arrested, highly viscous state into a fluid-like free flowing one with a low viscosity. The explanation of such a phase transition is that the van der Waals interaction between the particles becomes attractive at lower temperatures due to a temperature dependent change in dielectric constant. This macroscopic picture does not explain the observation that for some apolar solvents (like n-hexadecane) the transition is accompanied by a large calorimetric heat effect, while for others (e.g. benzene and CCl_4) it is not.

From SFS data (Fig. 5) on dispersions in arrested, low temperature states and fluidic high temperature states it can be observed that for n-hexadecane the surface state changes from a well ordered crystalline-like layer to a disordered chaotic surface. The molecular orientation of the surface bound chains with respect to the surface normal is 52° , which can be obtained using Eqs. 9, 10 and 2 on spectra taken with polarization combinations *ppp*, *ssp*, and *sps*. For solvents that do not display a heat effect it can be observed that the particle surface structure in both the arrested and fluidic states is disordered. The transition between a well ordered surface state and a disordered one costs energy that can be inserted in the system by means of heat. Because n-hexadecane has a similar

conformation as the surface grafted films, it can intercalate with the surface chains and hence form a nicely ordered, crystalline-like film. The formation of such a film explains the poorly understood discrepancy in the observed heat effects: In fluid suspension in n-hexadecane at high temperatures, the interfacial molecules are in a liquid-like state of conformational disorder. As the temperature is lowered, the onset of gelation is identified by macroscopic phenomena, including changes in turbidity, heat release, and diverging viscosity. At the molecular level, the onset of gelation coincides with straightening of the carbon-carbon backbones of the interfacial molecules and the formation of an ordered layer of both solvent molecules and surface-grafted molecules. Solvents such as benzene that cannot intercalate with the surface-grafted chains, do not interact strongly with the chains on the particle surface and therefore no heat is released upon cooling [57].

4.1.2 Gel formation

A related interesting surface effect occurs when a suspension of 123 nm particles is prepared in n-hexadecane and quenched below the gelation point. After 2 mins. the dispersion is already in an arrested state (as can be observed from the pictures on the left side of the graph). However, SFS spectra show that the formation of an ordered surface layer is a process that takes place on the timescale of several days. Fig. 6 shows several spectra as a function of time. It can be seen that the relative amplitude of the symmetric CH_3 and CH_2 stretch modes change dramatically, which is indicative of the slow formation of an ordered film [58]. Further experiments indicate that there may be a dependence on particle size. The origin of this behavior could be correlated to surface freezing, but the exact mechanism is not yet clarified.

4.2 Electrostatically stabilized systems

Colloidal soft matter systems that are stabilized by electrostatic interactions typically occur in aqueous environments. Although the generation of SH photons from surfaces of micron-sized particles has been reported already in the 1980's [59], it is only since 1996 [60] that SHS experiments have been performed on colloidal systems with the aim of monitoring surface properties. It has convincingly been shown that it is possible to follow adsorption kinetics of solvated molecules at particle

interfaces. Since the SHS amplitude increases with the number of adsorbed molecules an isotherm can be produced. With such measurements it is possible to determine the Gibbs adsorption energy [61], or to get access to the adsorption model [62, 63]. Much of this work has been reviewed by Eisenthal [64].

SHS has also been used to probe vesicle-membrane and emulsion properties. An example from Ref. [65] is given in Fig. 7. It shows the transport of malachite green ions (MG^+) through a liposome membrane. Initially, the electronically resonant SH intensity is low since there are few surface charges. After addition of MG^+ ions to the solution the potential increases and then drops off as MG^+ ions cross the liposome membrane and reach an equilibrium position. Upon addition of Gramicidin A, a compound that facilitates ionic transport in cell membranes, steady state can be reached with more MG^+ ions on the inside of the membrane.

Also it is possible to relate the SH intensity to the surface potential and charge [66]. Ions create or change the electric double layer potential around a particle or droplet in solution. Thus, apart from the incoming laser fields the molecules at the surface and in the surroundings of the double layer experience a DC field (\mathbf{E}_{DC}) as well. As a consequence the polarization (see Eq. (1)) may acquire an additional term of the form: $\chi_{ijkl}^{(3)}(\omega_1 + \omega_2)\mathcal{E}_{1,j}(\omega_1)\mathcal{E}_{2,k}(\omega_2)\mathcal{E}_{l,DC}$ (where $\chi^{(3)}$ is the third-order bulk-allowed optical susceptibility) so that it is now a measure of surface structure effects and charge effects in the bulk of the electric double layer region. In SHS and SFS experiments both effects are measured. SHS has also been applied to study changing membrane fluidity of liposomes by monitoring the scattered SH intensity of malachite green as a function of cholesterol [67], and ionic strength [68].

Since water has a high absorption coefficient for infrared radiation, vibrational SFS experiments in water are more involved than similar SHS experiments, but they can be performed. Thanks to the advances made in the development of pulsed infrared laser sources combined with the notion that it is possible to perform pump-probe experiments with femtosecond infrared pulses in bulk water (see e.g. [69]) and on water surfaces (see e.g. [70, 71]) it is likely that in the near future SFS experiments can be performed routinely in aqueous environment. As a consequence it will be possible to probe in-situ and label-free the molecular structure, orientation, chirality, molecular ordering and chemical changes at aqueous interfaces of colloids, nanoscopic emulsion droplets and liposomes.

5 Interfacial molecular structure of solid/solid dispersions

Another interesting development is the application of SHS and SFS to probe the properties of heterogeneities in solid compounds. SHS has been used to probe the surfaces of embedded Si nanocrystals in a glass matrix [72]. SFS has been employed to measure the size and optical properties of buried crystalline domains in poly(lactic acid) microspheres [73]. This application enabled us to obtain insight in the structure and functionality of a newly developed medicinal compound for liver cancer treatment that is based on the use of biodegradable polymer as a matrix [74]. Due to the high sensitivity [75] of these methods for ordered structures, they are also interesting for the detection of small quantities of protein crystal [76].

6 Conclusions and outlook

It is clear that currently a number of exciting developments are taking place that allow for a detailed observation of molecular structure, chirality, local charge, order and orientation at soft matter interfaces with increasing complexity. The possibility to exclusively measure in-situ and non-invasively the influence of changing composition, pH, temperature and ion content on the molecular surface properties is an important development.

It is now also possible to measure molecular interfacial properties of colloidal soft matter systems, without the need to resort to planar model systems or fluorescent labelling. Such systems have a relative surface area that is orders of magnitude bigger than that of planar interfaces. Exclusively observing chemical properties and changes in a molecular layer of a few molecular dimensions thick around a small particle or droplet in liquid phase adds a new dimension to the field of surface science. We can start to explore the detailed molecular mechanisms behind diverse processes such as (e.g.) vesicle fusion, emulsion stabilization, and colloidal self-assembly or particle synthesis.

7 Acknowledgements

This work is part of the research programme of the Max-Planck Society.

Table 1: References describing various models for SHS and SFS. Their limitations are also given.

m is the ratio of the refractive index of the particle and the surrounding medium.

Model	limit	SHS	SFS
RGD	$ m - 1 \ll 1$ or: $\frac{4\pi R m-1 }{\lambda} \ll 1$	[77–83]	[52, 54, 84]
WKB	$ m - 1 < 1$	[83]	[52]
Small particle	$qR \ll 1$	Metal [85–87] Dielectric [82, 88–91] cylinder [83]	[52]
Mie theory	Exact for spherical particles	[92–95]	[96]

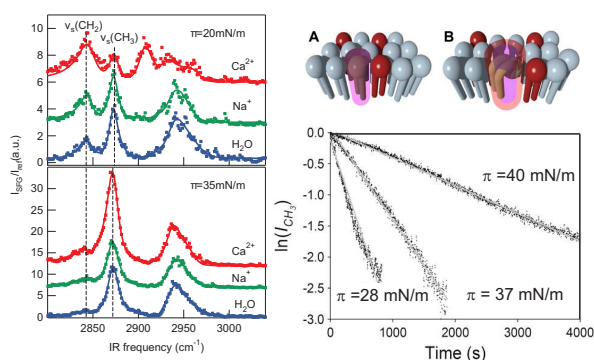


Figure 1: Left: Ca^{2+} ions influence the composition of a phospholipid monolayer on top of water. A high relative ratio of the signal of the symmetric CH_3 and CH_2 vibrational modes (marked by the dashed line) is indicative of an ordered monolayer. At low phospholipid densities (top traces), Ca^{2+} ions reduce order, while at high phospholipid densities (bottom traces), Ca^{2+} ions increase order with respect to a monolayer on water or monovalent salt solution. Adapted from [40]. Copyright ACS. Right: Decay of the SFG signal of the symmetric methyl stretch mode in phospholipid bilayers, indicative of flip-flop rate. Bilayers prepared with low surface density have a higher flip-flop rate than those prepared at a high surface density. From these measurements the activation area of the flip-flop process was determined to be 73 \AA^2 . The top panel displays the area of a phospholipid in the ground state (purple) and in its most unfavorable conformation (orange). Adapted from [45]. Copyright Biophysical Society.

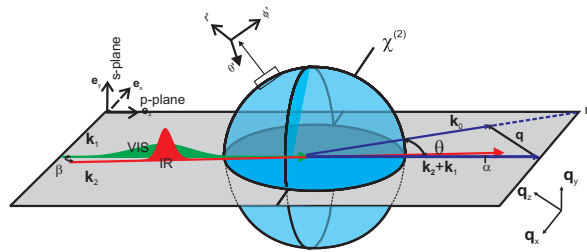


Figure 2: Illustration of the in-plane scattering geometry for SFS experiments, indicating the k -vectors of the incoming beam (k_1 and k_2) and the scattered sum frequency beam (k_0), the scattering wave vector (q), and the scattering angle (θ). β is the angle between k_2 and k_1 and α is the angle between k_2 and $k_1 + k_2$. Beams polarized parallel to the plane of incidence are defined as p -polarized, while beams with an oscillating field in the y -direction are indicated as s -polarized. The direction $k_1 + k_2$ is called the forward direction ($\theta=0$).

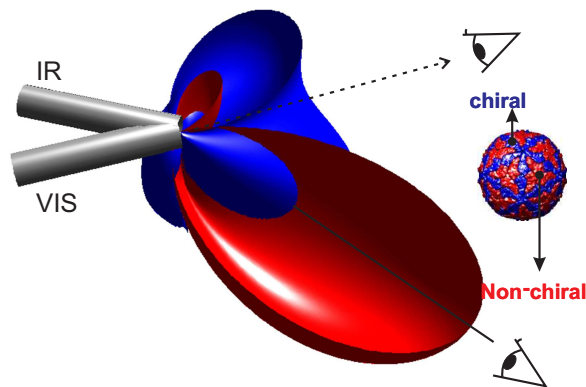


Figure 3: Three dimensional image of calculated sum frequency scattering pattern of a 200 nm particle (which e.g. could be a virus capsid) containing both chiral (blue) and non-chiral (red) groups. It can be seen that both groups generate a distinctly different scattering pattern that points in different directions, so that they can be measured separately.

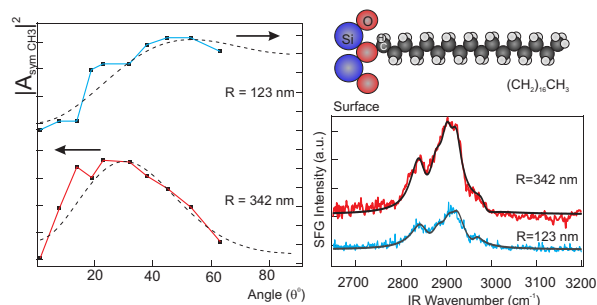


Figure 4: Left: Scattering patterns (obtained in *ppp* polarization) of sterically stabilized colloidal particles with radii (R) of 123 nm and 342 nm, dispersed with 5 v.v.% in CCl_4 . Right: Spectra obtained at $\theta=26^\circ$ for particles with different size. An illustration of the surface bound stearyl groups is also shown. Adapted from [52], copyright APS.

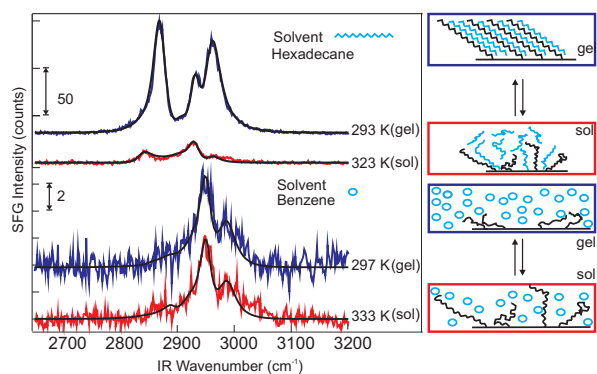


Figure 5: The highly viscous gel state of a colloidal dispersion transforms into a liquid like one upon increase of temperature. This process happens for stearyl-coated silica particles dispersed in hexadecane and benzene. Sum frequency scattering spectra ($\theta=51^\circ$) of the highly viscous gel state (293 K) and the liquid like suspension (333 K) of colloids dispersed in hexadecane (top traces) and benzene (bottom traces). The corresponding surface state of the particle interfaces as determined from the spectra are completely different and can be explained by surface-solvent interactions as displayed on the right. From [57], copyright IOP.

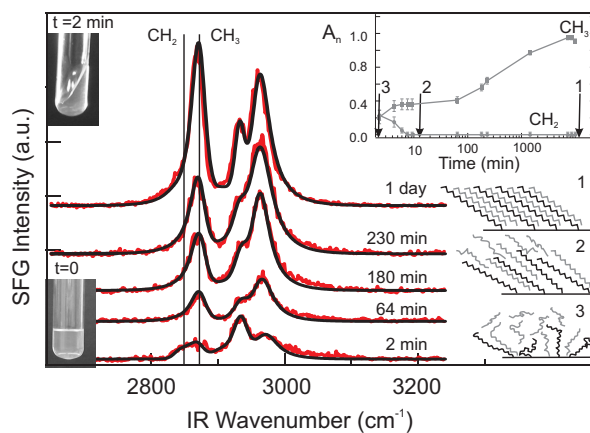


Figure 6: Temporal evolution of the colloidal surface after gelation. SFS spectra (gray lines, *ppp* polarization) of a 24 v. v. % gel as a function of gel age as indicated. The structure of the boundary layer is schematically depicted for the three most relevant time intervals during gel formation and aging. From [58].

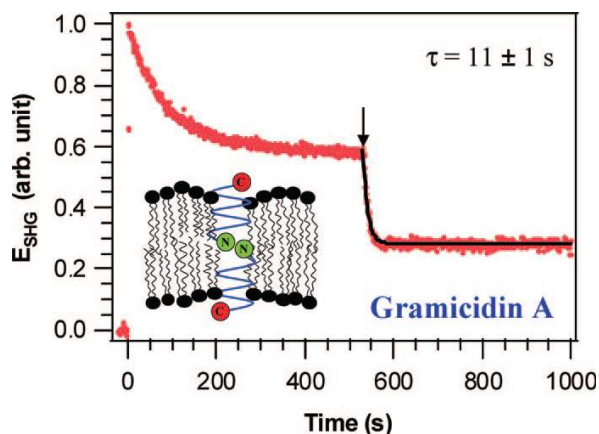


Figure 7: Square root of SHS intensity as a function of time before and after addition of gA. MG^+ is added to a lipid (DOPG) solution at $t=0$ s. The arrow indicates the time at which Gramicidin A is introduced into the MG^+ -liposome solution. The solid black lines represent a single exponential fit to the data. From [65], copyright ACS.

References

- [1] Sackmann, E. *Science* **271**, 43–48 (1996).

- [2] Adamson, A. W. and Gast, A. P. *Physical chemistry of surfaces*. Wiley-interscience, (1997).
- [3] Shen, Y. R. *Nature* **337**, 519 (1989).
- [4] Butcher, P. N. and Cottor, D. *The Elements of Nonlinear Optics*. Cambridge University Press, (1990).
- [5] Bain, C. D. *J. Chem. Soc., Faraday Trans.* **91**, 1281 – 1296 (1995).
- [6] Jie Wang, Xiaoyun Chen, M. L. C. and Chen, Z. *PNAS* **102**, 4978–4983 (2005).
- [7] Lambert, A. G., Davies, P. B., and Neivandt, D. J. *Appl. Spectr. Rev.* **40**, 103–144 (2005).
- [8] Guyot-Sionnest, P., Hunt, J. H., and Shen, Y. R. *Phys. Rev. Lett.* **59**(14), 1597–1600 (1987).
- [9] Harris, A. L., Chidsey, C., Levinos, N., and Loiacona, D. *Chem. Phys. Lett.* **141**, 350–356 (1987).
- [10] Heinz, T. F. *Nonlinear surface electromagnetic phenomena*, chapter 5. Elsevier, New York (1991).
- [11] Shen, Y. R. *Surf. Sci.* **299/300**, 551–562 (1994).
- [12] Bloembergen, N. *Appl. Phys. B* **68**, 289–293 (1999).
- [13] Bonn, M., Hess, C., Funk, S., Miners, J. H., Persson, B. N. J., Wolf, M., and Ertl, G. *Phys. Rev. Lett.* **84**, 4653–4656 (2000).
- [14] Kubota, J. and Domen, K. *Anal Bioanal Chem.* **388**, 17–27 (2007).
- [15] Vidal, F. and Tadjeddine, A. *Rep. Prog. Phys.* **68**(5), 1095–1127 (2005).
- [16] Chen, Z., Shen, Y. R., and Somorjai, G. A. *Annu. Rev. Phys. Chem.* **53**, 437–465 (2002).
- [17] Raschke, M. B. and Shen, Y. R. *Curr. Opin. Solid State Mater Sci.* **8**, 343–352 (2004).
- [18] Eisenthal, K. B. *Chem. Rev.* **96**(4), 1343–1360 (1996).
- [19] Richmond, G. L. *Chem. Rev.* **102**, 2693–2724 (2002).

- [20] Shultz, M. J., Schnitzer, C., Simonelli, D., and Baldelli, S. *Int. Rev. Phys. Chem.* **19**(1), 123–153 (2000).
- [21] Richmond, G. L. *Annu. Rev. Phys. Chem.* **52**, 357–389 (2001).
- [22] Shultz, M., Baldelli, S., Schnitzer, C., and Simonelli, D. *J. Phys. Chem. B* **106**, 5313–5324 (2002).
- [23] Sioncke, S., Verbiest, T., and Persoons, A. *Mater. Sci. Eng.* **42**, 115–155 (2003).
- [24] Simpson, G. J. *Chem. Phys. Chem.* **5**(9), 1301–1310 (2004).
- [25] Belkin, M. A. and Shen, Y. R. *Int. Rev. Phys. Chem.* **24**, 257–299 (2005).
- [26] Oh-e, M., Yokoyama, H., Yorozuya, S., Akagi, K., Belkin, M. A., and Shen, Y. R. *Phys. Rev. Lett.* **93**(26), 267402 (2004).
- [27] Dreesen, L., Sartenaer, Y., Humbert, C., Mani, A. A., Lemaire, J. J., Methivier, C., Pradier, C. M., Thiry, P. A., and Peremans, A. *Thin Solid Films* **464-65**, 373–378 (2004).
- [28] Dreesen, L., Sartenaer, Y., Humbert, C., Mani, A. A., Methivier, C., Pradier, C. M., Thiry, P. A., and Peremans, A. *ChemPhysChem* **5**(11), 1719–1725 (2004).
- [29] Chen, X. Y., Clarke, M. L., Wang, J., and Chen, Z. *Int. J. Mod. Phys.* **19**(4), 691–713 (2005).
- [30] Chen, X. Y., Tang, H. Z., Even, M. A., Wang, J., Tew, G. N., and Chen, Z. *J. Am. Chem. Soc.* **128**(8), 2711–2714 (2006).
- [31] Stokes, G. Y., Gibbs-Davis, J. M., Boman, F. C., Stepp, B. R., Condie, A. G., Nguyen, S. T., and Geiger, F. M. *J. Am. Chem. Soc.* **129**, 7492–7493 (2007).
- [32] Sartenaer, Y., Tourillon, G., Dreesen, L., Lis, D., Mani, A. A., Thiry, P. A., and Peremans, A. *Biosens. Bioelectr.* **22**(9-10), 2179–2183 (2007).
- [33] Wurpel, G. W. H., Sovago, M., and Bonn, M. *J. Am. Chem. Soc.* **129**, 8420–8421 (2007).
- [34] Roke, S., Schins, J. M., Müller, M., and Bonn, M. *Phys. Rev. Lett.* **90**(12), 128101 (2003).

- [35] Liu, J. and Conboy, J. C. *J. Am. Chem. Soc.* **126**, 8376–8377 (2004).
- [36] Bonn, M., Roke, S., Berg, O., Juurlink, L. B. F., Stamouli, A., and Muller, M. *J. Phys. Chem. B* **108**(50), 19083–19085 (2004).
- [37] Ma, G. and Allen, H. C. *Langmuir* **22**(12), 5341–5349 (2006).
- [38] Ma, G. and Allen, H. C. *Langmuir* **23**(2), 589–597 (2007).
- [39] Liu, J. and Conboy, J. C. *J. Phys. Chem. C* **111**, 8988–8999 (2007).
- [40] Sovago, M., Wurpel, G. W. H., Smits, M., Muller, M., and Bonn, M. *J. Am. Chem. Soc.* **129**, 11079–11084 (2007).
- [41] Kim, J. and Somorjai, G. A. *J. Am. Chem. Soc.* **125**(10), 3150–3158 (2003).
- [42] Chen, X. Y., Wang, J., Sniadecki, J. J., Even, M. A., and Chen, Z. *Langmuir* **21**(7), 2662–2664 (2005).
- [43] Chen, X. Y., Wang, J., Paszti, Z., Wang, F. L., Schrauben, J. N., Tarabara, V. V., Schmaier, A. H., and Chen, Z. *Anal. Bioanal. Chem.* **388**(1), 65–72 (2007).
- [44] Chen, X. Y., Wang, J., Boughton, A. P., Kristalyn, C. B., and Chen, Z. *J. Am. Chem. Soc.* **129**(5), 1420–1427 (2007).
- [45] Anglin, T. C. and Conboy, J. C. *Biophys. J.* **95**, 186 – 193 (2008).
- [46] Wang, J., Lee, S. H., and Chen, Z. *J. Phys. Chem. B* **112**(7), 2281–2290 (2008).
- [47] Johnson, C. M. and E., T. *Phys. Chem. Chem. Phys.* **7**, 2635–3641 (2005).
- [48] Sugiharto, A. B., Johnson, C. M., de Aguiar, H. B., Aloatti, L., and Roke, S. *Appl. Phys. B* **91**, 315–318 (2008).
- [49] Sugiharto, A. B., Johnson, C. M., Dunlop, I. E., and Roke, S. *J. Phys. Chem. C* **112**, (Letter) 7531–7534 (2008).
- [50] Baldelli, S. *ChemPhysChem* **9**, 2291–2298 (2008).

- [51] Landau, L. D. and Lifshitz, E. M. *Electrodynamics of continuous media*. Pergamon press, Oxford, (1960).
- [52] Roke, S., Bonn, M., and Petukhov, A. V. *Phys. Rev. B* **70**, 115106 (2004).
- [53] Kerker, M. *The scattering of light and other electromagnetic radiation*. John Wiley and sons, New York, (1969).
- [54] de Beer, A. G. F. and Roke, S. *Phys. Rev. B* **75**, 245438–1 –245438–8 (2007).
- [55] Dadap, J. I., de Aguiar, H. B., and Roke, S. *submitted to J. Chem. Phys.* (2009).
- [56] van Helden, A. K., Jansen, J. W., and Vrij, A. *J. Colloid Interface Sci.* **81**, 354–368 (1981).
- [57] Roke, S., Buitenhuis, J., van Miltenburg, J. C., Bonn, M., and van Blaaderen, A. *J. Phys.-Condens Matter* **17**(45), S3469–S3479 (2005).
- [58] Roke, S., Berg, O., Buitenhuis, J., van Blaaderen, A., and Bonn, M. *Proc. Nat. Acad. Sci.* **103**(36), 13310–13314 (2006).
- [59] Murphy, D. V., von Raben, K. U., Chang, R. K., and Dorain, P. B. *Chem. Phys. Lett.* **85**, 43–47 (1982).
- [60] Wang, H., Yan, E. C. Y., Borguet, E., and Eissenthal, K. B. *Chem. Phys. Lett.* **259**(1-2), 15–20 (1996).
- [61] Wang, H. F., Yan, E. C. Y., Liu, Y., and Eissenthal, K. B. *J. Phys. Chem. B* **102**, 4446–4450 (1998).
- [62] Campen, R. K., Zheng, D. S., Wang, H. F., and Borguet, E. *J. Phys. Chem. C* **111**, 8805–8813 (2007).
- [63] Wang, J., Paszti, Z., Clarke, M. L., Chen, X. Y., and Chen, Z. *J. Phys. Chem. B* **111**(21), 6088–6095 (2007).
- [64] Eissenthal, K. B. *Chem. Rev.* **106**(4), 1462–1477 (2006).
- [65] Liu, J., Subir, M., Nguyen, K., and Eissenthal, K. B. *J. Phys. Chem. B* **112**, 15263–15266 (2008).

- [66] Yan, E. C. Y., Liu, Y., and Eisenthal, K. B. *J. Phys. Chem. B* **102**, 6331–6336 (1998).
- [67] Yan, E. C. Y. and Eisenthal, K. B. *Biophys. J.* **79**(2), 898–903 (2000).
- [68] Shang, X. M., Liu, Y., Yan, E., and Eisenthal, K. B. *J. Phys. Chem. B* **105**(51), 12816–12822 (2001).
- [69] Bakker, H. J. *Chem. Rev.* **108**, 1456–1473 (2008).
- [70] McGuire, J. A. and Shen, Y. R. *Science* **313**(5795), 1945–1948 (2006).
- [71] Smits, M., Ghosh, A., Sterrer, M., Mueller, M., and Bonn, M. *Phys. Rev. Lett.* **98**, 098302 (2007).
- [72] Jiang, Y., Wilson, P. T., Downer, M. C., White, C. W., and Withrow, S. P. *App. Phys. Lett.* **78**, 766–768 (2001).
- [73] de Beer, A. G. F., de Aguiar, H. B., Nijsen, J. W. F., and Roke, S. *Phys. Rev. Lett.* **102**, 095502–1–4 (2009).
- [74] de Aguiar, H. B., Nijsen, J. F. W., and Roke, S. *in preparation* (2009).
- [75] de Aguiar, H. B. and Roke, S. *in preparation* (2009).
- [76] Wampler, R. D., Kissick, D. J., Dehen, C. J., Gualtieri, E. J., Grey, J. L., Wang, H. F., Thompson, D. H., Cheng, J. X., and Simpson, G. J. *J. Am. Chem. Soc.* **130**(43), 14076–14078 (2008).
- [77] Martorell, J., Vilaseca, R., and Corbalan, R. *Phys. Rev. A* **55**, 4520–4525 (1997).
- [78] Brudny, V. L., Mendoza, B. S., and Mochán, W. L. *Phys. Rev. B* **62**, 11152–11162 (2000).
- [79] Yang, N., Angerer, W. E., and Yodh, A. G. *Phys. Rev. Lett.* **87**(10), 103902–1–4 (2001).
- [80] Mochan, W. L., Maytorena, J. A., Mendoza, B. S., and Brudny, V. L. *Phys. Rev. B* **68**, 085318 (2003).
- [81] Brudny, V. L., Mochan, W. L., Maytorena, J. A., and Mendoza, B. S. *Phys. Stat. Sol. B* **240**(3), 518–526 (2003).
- [82] Dadap, J. I., Shan, J., and Heinz, T. F. *J. Opt. Soc. Am. B* **21**, 1328–1347 (2004).

- [83] Dadap, J. I. *Phys. Rev. B* **78**, 205322–1–18 (2008).
- [84] Roke, S., Roeterdink, W. G., Wijnhoven, J. E. G. J., Petukhov, A. V., Kleyn, A. W., and Bonn, M. *Phys. Rev. Lett.* **91**(25), 258302 (2003).
- [85] Agarwal, G. S. and Jha, S. S. *Phys. Rev. B* **26**(2), 482–496 (1982).
- [86] Hua, X. M. and Gersten, J. I. *Phys. Rev. B.* **33**, 3756 (1986).
- [87] Nappa, J., Revillod, G., Russier-Antoine, I., Benichou, E., Jonin, C., and Brevet, P. F. *Phys. Rev. B.* **71**, 165407 (2005).
- [88] Dadap, J. I., Shan, J., Eisenthal, K. B., and Heinz, T. F. *Phys. Rev. Lett.* **83**(20), 4045–4048 (1999).
- [89] Makeev, E. V. and Skipetrov, S. E. *Opt. Commun.* **224**(1-3), 139–147 (2003).
- [90] Figliozzi, P., Sun, L., Jiang, Y., Matlis, N., Mattern, B., Downer, M. C., Withrow, S. P., White, C. W., Mochán, W. L., and Mendoza, B. S. *Phys. Rev. Lett.* **94**, 047401 (2005).
- [91] Shan, J., Dadap, J. I., Stiopkin, I., Reider, G. A., and Heinz, T. F. *Phys. Rev. A* **73**(2), 023819 (2006).
- [92] Hayata K.; Koshiba, M. *Phys. Rev. A* **46**, 6104–6107 (1992).
- [93] Oestling, D., Stampfli, P., and Bennemann, K. *Z. Phys. D* **28**, 169–175 (1993).
- [94] Dewitz, J. P., Hubner, W., and Bennemann, K. H. *Z. Phys. D.* **37**(1), 75–84 (1996).
- [95] Pavlyukh, Y. and Huebner, W. *Phys. Rev. B* **70**, 245434 (2004).
- [96] de Beer, A. G. F. and Roke, S. *Phys. Rev. B* **79**, 155420–1–9 (2009).